Design of TEM Transmission Line for Probe Calibration up to 40 GHz

Morten Sørensen*, Shubhankar Marathe*, David Pommerenke*, Hamed Kajbaf†, Jin Min†
*EMC Laboratory
Missouri University of Science and Technology
Rolla, Missouri, USA
Email: sorensenmo, skmcr4, davidjp@mst.edu
†Amber Precision Instruments
San Jose, California, USA hamed, jinmin@amberpi.

***Abstract*—With the ongoing development of 5G wireless communication, frequencies as high as 40 GHz have become relevant for EMI near-field scanning. This paper describes the development process of two transmission lines with air dielectrics for probe calibration, namely a rod over ground plane and an air trace. Because of homogeneous dielectrics the transmission lines become almost pure TEM, which is preferable regarding probe calibration to a coplanar waveguide (quasi-TEM). The design process shows that at very high frequencies, transitions in the transmission line are critical and all small physical details must be included in the simulation model in order for it to be reliable.**

I. Introduction

Phase-resolved near-field scanning (NFS) has been widely used in electromagnetics and antenna research for many years. With the ongoing development of 5G wireless communication, mm wavebands above 20 GHz are being intensively studied [1], [2] and there is a great need for high frequency probes and calibration of them. In most EMC near-field scanning systems, a probe (or a set of probes) captures a large set of near-field data on a surface plane close to the device under test (DUT). For example, an E-field probe [3] or an H-field probe [4] can be used to visualize the E-field or the H-field near-field distribution over a DUT.

Various probe calibration methods suitable for different frequency ranges are published in the literature; the different calibration methods and their typical frequency ranges are mentioned in the IEEE Std 1309-2013 [5] and IEC 61000-4-20 Annex E covers E-field probe calibration in TEM waveguides [6].

Previous work [7] has shown that referring a measured voltage to the known fields of a 50 Ω transmission line (TL) is an effective method for calculating the probe factor. If the measurements are done with a Vector Network Analyzer (VNA) (see Fig. 1), the probe factor (PF) is given by:

$$PF = \frac{ref}{S_{21}} \tag{1}$$

where *ref* is the normalized near-field strength (*E* or *H*) from a simulation at a given input voltage and at a given height above the TL:

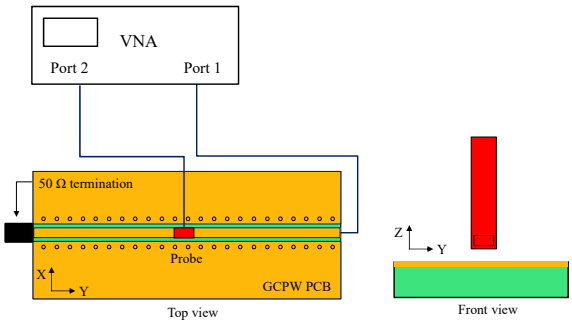

Fig. 1: A typical set-up for probe calibration by way of a coplanar waveguide and a VNA.

$$ref = \frac{Near\text{-}field_{\text{simulation}}}{V_{\text{simulation}}} \tag{2}$$

A pure TEM mode is convenient for calibration since pure TEM is frequency independent and the field components are well defined. But of course no physical case is pure TEM because it would require infinite conductivity and transitions, e.g., from connector to transmission line, will cause some non-TEM mode. In the imperfect physical world, the features of the transmission line for calibration could be prioritized as follows:

1) Well defined field component, i.e., the near-field must be orthogonal to the propagation and there should be no tangential component.
2) The near-field amplitude along a line across the TL must be as frequency independent as possible.
3) Impedance match in order to avoid reflections. If reflections arise, the calibration probe can measure the field along the line and relate the average to the average in the simulation.

A simple microstrip can be used up to a few GHz [8], [9] while a grounded coplanar waveguide (CPW) is better for higher frequencies [10]. Unfortunately, the inhomogeneous medium of a CPW causes non-TEM behavior [11] which is illustrated in Section III-C. Calibration becomes more difficult

with non-TEM modes (e.g., frequency dependent) and inaccurate because of the tangential field component. The purpose of this study was to design a structure that comes close to pure TEM.

This paper goes through the design process of two transmission lines in air, i.e., homogeneous dielectric. In Section II the design models are described. The first method was a rod above a ground plane (Section II-A), while the second method was an easier to manufacture air trace (Section II-B). Simulation and measurement results for the two design models are presented and discussed in Section III.

The calibration process depends entirely on the reliability of the simulations. Hence, Section III-A1 gives an example of the gap between simulations and measurements and how to bridge it. In Section IV, suggestions for further improvements are discussed. Finally conclusions are drawn in Section V.

II. Design Models

A. First Structure: Rod over Ground

A rod in air over a ground plane results in true TEM because of the non-dispersive dielectric. A 30 mm long rod was soldered with a 2.4 mm connector to a 0.203 mm thick by 1.27 cm long CPW from Southwest. An aluminum structure was machined as the ground plane. The distance between the rod and the ground plane was carefully tuned to 0.16 mm so that the impedance was 50 Ω, as shown in Fig. 2.

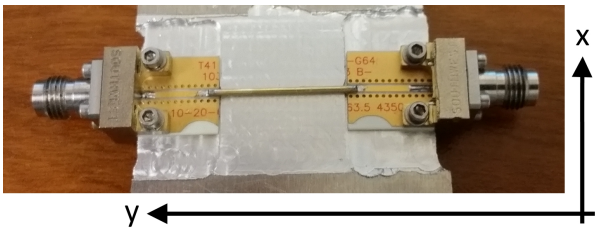

Fig. 2: The rod over ground plane.

B. Second Structure: Air Trace

A 2.4 mm Southwest connector was attached to 1 mm thick GPW with a 1 mm wide trace. The trace continues in an air trace which was made by a cutout slot in a PCB plated with copper. With carefully tuning of the distances, a 50 Ω transmission lines with low loss and almost pure TEM was obtained, as shown in Fig. 3. The advantage of this structure is it can be PCB manufactured and man-made craftsmanship is avoided. However, in PCB manufacturing the slot will be completely plated and the trace will be short circuited to ground. Hence, it is necessary manually to drill away the plating.

C. Simulations Models

The two transmission lines were simulated in CST Microwave Studio with the time domain (FIT) solver. Input power was normalized to 1 W. The number of mesh cells were 8 million for the rod over ground plane and 6 million for the

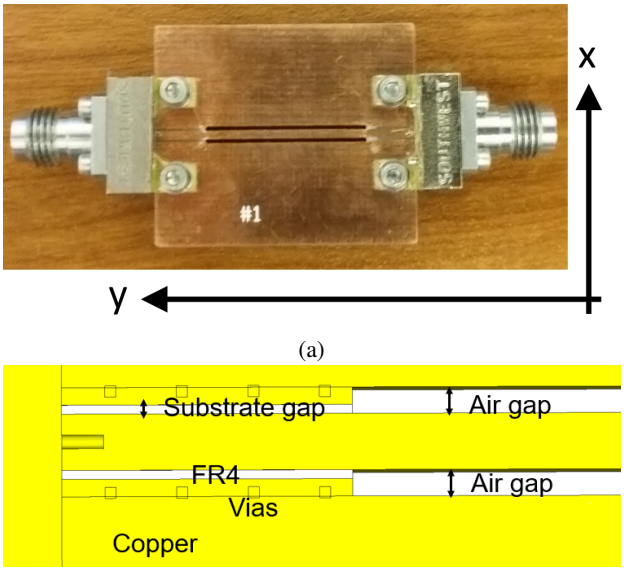

Fig. 3: The air trace. (a) Air trace with Southwest connector (b) The trace is separated from ground by milling the plating away at the end of slots and by making a cut in the trace at the backside.

air trace. The Southwest connector was included in the model as shown in Fig. 4. The model was excited with a waveguide port to the coaxial inner part of the connector with a diameter of 1.61 mm.

III. Results and Discussion

Based on the desired features described in Section I, the calibration structure was evaluated with respect to the tangential field component (non-TEM mode), S-parameters, and amplitude across and along the trace. Time domain reflectometry (TDR) was used in measurements to analyze imperfections in the structure. The near-field was evaluated 1 mm above the TL, which is a typical scanning height for high frequency (up to 40 GHz) applications.

A. First Structure: Rod over Ground

The simulations results for the rod over ground are shown in Fig. 5 and Fig. 6. At a glance, the structure looks very promising. Fig. 5 shows that the orthogonal field across the rod is frequency independent up to 20-30 GHz while the curve shape starts to change and the amplitude starts to decrease approaching 40 GHz. The tangential field is very weak compared to the orthogonal field at all points across the rod so the non-TEM mode will not perpetuate the calibration. Fig. 6 shows that standing waves cause variation of the orthogonal field along the rod, which increases with frequency (up to 6 dB at 40 GHz) so it will be necessary to find the average field strength along the trace. The reflections are caused by both the transition from connector to CPW and the transition from CPW to rod. A simulation of the connector and CPW alone showed variations along the rod up to 3 dB at 40 GHz. Fig. 6

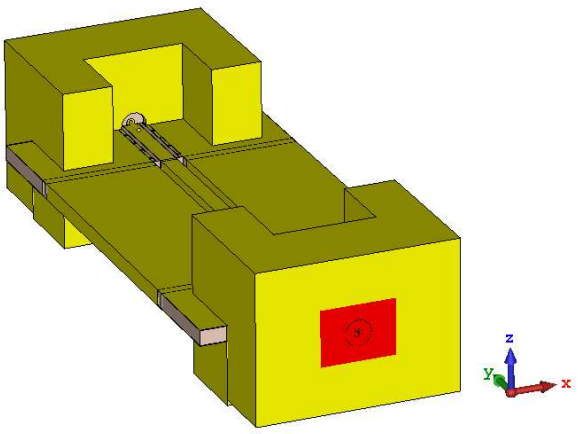

(a) CST model of the air trace.

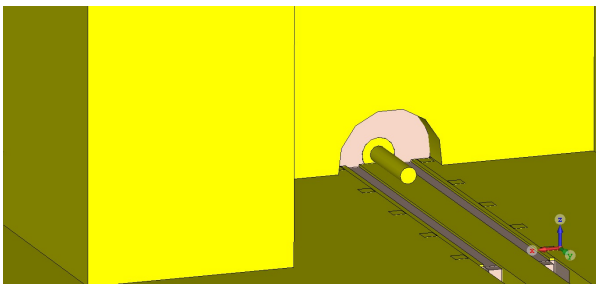

(b)

Fig. 4: Numerical model. (a) Air trace with Southwest connector (b) Transition from Southwest connector to air trace.

also shows S_{11} for the port of the transmission line and S_{21} between the two ports of the transmission line. S_{21} decreases as S_{11} increases. It seems that mismatch is the reason for the S_{21} decrease with frequency.

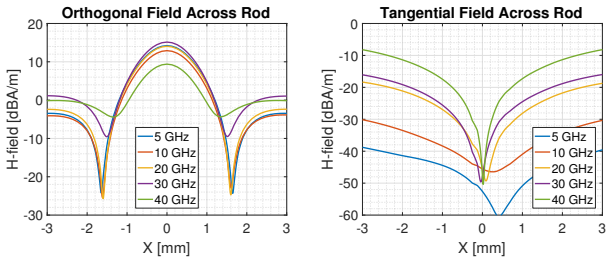

Fig. 5: Orthogonal and tangential field across the rod.

1) Bridging the gap Between Measurement and Simulations: H-field and S-parameters for the rod over ground were also measured. At first, there were large differences between the simulations and measurements. The variation along the trace was larger and the power transmitted from port 1 to port 2 (S_{21}) was much lower in the measurements compared to the simulations. As an example, the comparison of S_{21} is shown in Fig. 7. The physical and numerical models were compared in details and minor differences were observed. The three main

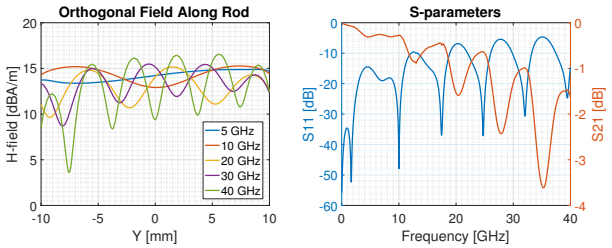

Fig. 6: Left: Orthogonal field along the rod. Right: S-parameters.

courses for the gap between simulations and measurements were in the following order, shown in Fig. 8:

1) Surface roughness on the machined ground plane causing large resistive loss.
2) Gap between CPW and machined ground plane causing further reflections and causing power to disappear as radiation.
3) Distance from end of CPW to first ground via causing further reflections and causing power to disappear as radiation.

The details were refined in the simulation and better agreement between simulations and measurement was obtained, as shown in Fig. 7.

Imperfections 2 and 3 in the physical model were corrected with silver paint, hence, the loss was lowered and standing waves on the rod were reduced. Surface roughness could easily be removed, but since the structure requires precise craftsmanship it was decided to choose a structure which could benefit from PCB manufacturing, namely the air trace.

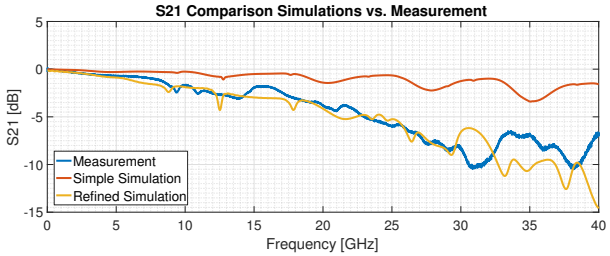

Fig. 7: Comparison between simulation and measurements of S_{21}.

B. Second Structure: Air Trace

In Fig. 9 and Fig. 10 the simulation results of the air trace are shown. Again, the structure seems promising up to 30 GHz. Orthogonal fields across the trace are frequency independent up to 25-30 GHz, but the curve shape and amplitude change as frequency approaches 40 GHz. The tangential field is negligible. Fig. 10 shows that standing waves become significant above 30 GHz (up to 7-8 dB at 40 GHz). Again, the reflections are caused by both the transition from connector to CPW and the transition from CPW to air trace. As frequency increases less power is transfered from port 1 to port 2 because of mismatch, dielectric loss and power radiated.

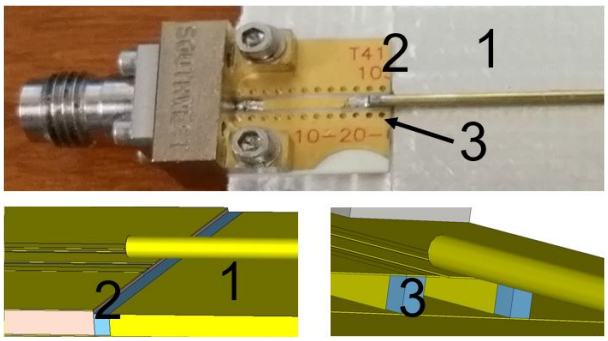

Fig. 8: The rod over ground plane. The 3 main courses for the gap between simulation and measurement are marked with numbers.

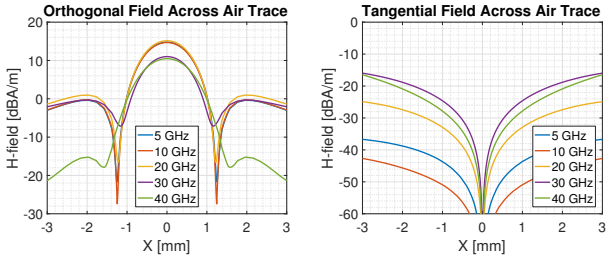

Fig. 9: Orthogonal and tangential field across the air trace.

1) Comparison Between Measurement and Simulations: Fig. 11 shows a comparison between simulations and measurements of S_{11} and S_{21}. Although there are differences in amplitude, there is good agreement regarding resonance frequencies and trends.

C. TEM vs. Non-TEM

As an illustration of the difference between the quasi-TEM behavior of a CPW and the more pure TEM of the air trace, the H-field across a 0.762 mm CPW is compared with the same field of the 1 mm thick air trace at 30 GHz. The H_y (tangential component) of the air trace is negligible compared the orthogonal field (H_x and H_z) at all points across the air trace. For the quasi-TEM CPW, the amplitude of the Hy component is comparable with the tangential components at x=-1 and x=1.

IV. Suggestions for Improvement

The measurement and simulations of the air trace revealed that the transition between CPW and air trace is very critical in order to avoid standing waves and loss. At 40 GHz the wavelength in free space is 7.5 mm. With a board thickness of 1 mm, the length of the detour the return current has to travel in the transition is more than 1/10 of the wavelength. Hence, this distance is comparable with the wavelength. One idea to overcome this problem is to make the board thinner. The air trace board was also designed with 0.8 mm and 0.6 mm thicknesses. Air and substrate gaps were adjusted to the thinner board in order to obtain 50 Ω.

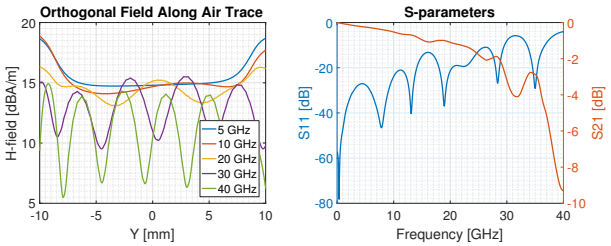

Fig. 10: Left: Orthogonal field along the air trace, Right: S-parameters.

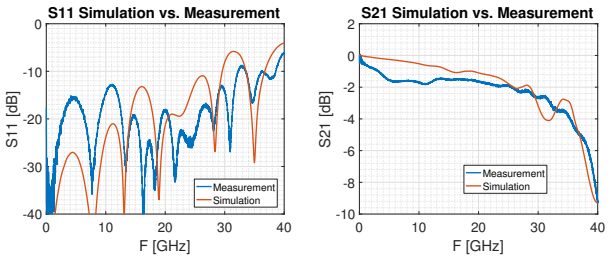

Fig. 11: Left: S_{11} simulation vs. measurement, Right: S_{21} simulation vs. measurement.

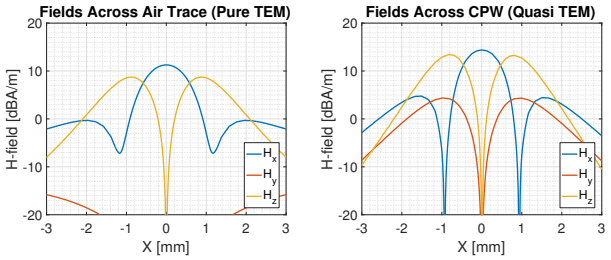

Fig. 12: Left: All three field components across the air trace, Right: All three field components across a CPW.

Fig. 13 shows both standing waves and loss are reduced with thinner boards. The variation along the trace at 30 GHz is reduced to approximately 3 dB for the 0.6 mm board corresponding to the reflections caused by the transition from Southwest connector to CPW.

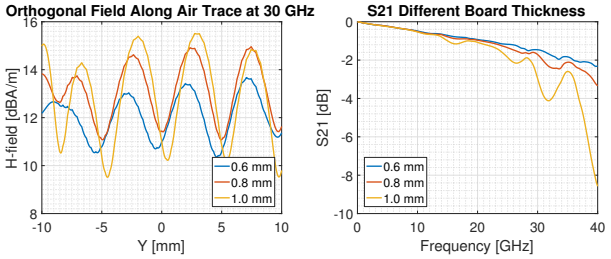

Fig. 13: Left: Standing waves are reduced with board thickness. Right: Loss is reduced with board thickness.

Another idea to overcome reflections could be to design attenuators along the line. But since there are two transitions in both ends i.e., connector to CPW and CPW to air trace, it

will require four attenuators causing a large reduction in the dynamic range.

V. Conclusion

Two different transmission lines in air (homogeneous dielectric) were designed for probe calibration up to 40 GHz: a rod over a ground plane and an air trace. Simulations and measurements show that it is possible to obtain almost pure TEM, but reflections and loss increase while the frequency approaches 40 GHz. This can be improved by decreasing the PCB thickness. However, it requires such small dimensions that PCB manufacturers are incapable of. The design study also made it clear that every physical detail must be included in the simulation in order to obtain good agreement. This is very important since the calibration method strongly depends on reliable simulations.

References

[1] T. S. Rappaport, G. R. MacCartney, M. K. Samimi, and S. Sun, "Wideband millimeter-wave propagation measurements and channel models for future wireless communication system design," *IEEE Transactions on Communications*, vol. 63, no. 9, pp. 3029–3056, Sept 2015.

[2] T. Wheeler, "Leading towards next generation "5G" mobile services," August 2015. [Online]. Available: https://www.fcc.gov/news-events/blog/2015/08/03/leading-towards-next-generation-5g-mobile-services

[3] G. Li, K. Itou, Y. Katou, N. Mukai, D. Pommerenke, and J. Fan, "A resonant e-field probe for rfi measurements," *IEEE Transactions on Electromagnetic Compatibility*, vol. 56, no. 6, pp. 1719–1722, Dec 2014.

[4] S. Shinde, S. Marathe, G. Li, R. Zoughi, and D. Pommerenke, "A frequency tunable high sensitivity h-field probe using varactor diodes and parasitic inductance," *IEEE Transactions on Electromagnetic Compatibility*, vol. 58, no. 1, pp. 331–334, Feb 2016.

[5] "IEEE standard for calibration of electromagnetic field sensors and probes (excluding antennas) from 9 khz to 40 ghz," *IEEE Std 1309-2013 (Revision of IEEE Std 1309-2005)*, pp. 1–111, Nov 2013.

[6] "Testing and measurement techniques – emission and immunity testing in transverse electromagnetic (tem) waveguides," *IEC 61000-4-20 Annex E*, 2010.

[7] J. Zhang, K. W. Kam, J. Min, V. V. Khilkevich, D. Pommerenke, and J. Fan, "An effective method of probe calibration in phase-resolved near-field scanning for emi application," *IEEE Transactions on Instrumentation and Measurement*, vol. 62, no. 3, pp. 648–658, March 2013.

[8] W. Liu, Z. Yan, and W. Zhao, "A study on calibration compensation and perturbation of electromagnetic probes," in *2017 7th IEEE International Symposium on Microwave, Antenna, Propagation, and EMC Technologies (MAPE)*, Oct 2017, pp. 195–199.

[9] M. A. Chahine, M. Khatib, A. Hami, R. Perdriau, and M. Ramdani, "Near field measurement system for the detection of electromagnetic field components radiated by microwave devices," in *2013 13th Mediterranean Microwave Symposium (MMS)*, Sept 2013, pp. 1–4.

[10] R. W. Jackson, "Coplanar waveguide vs. microstrip for millimeter wave integrated circuits," in *1986 IEEE MTT-S International Microwave Symposium Digest*, June 1986, pp. 699–702.

[11] S. Marathe, M. Soerensen, V. Khilkevich, D. Pommerenke, J. Min, and G. Muchaizde, "Effect of inhomogeneous medium on fields above gcpw pcb for near-field scanning probe calibration application," *IEEE Trans. Electromagn. Compat, Accepted for Publication*, 2018.